TIP-OVER RESPONSES OF HYDRAULIC MOBILE CRANES

R.F. Abo-Shanab
Department of Mechanical Engineering
University of Assiut, Egypt

N. Sepehri
Department of Mechanical and Manufacturing Engineering
University of Manitoba, Winnipeg, Manitoba, Canada R3T-5V6
Corresponding Author: nariman@cc.umanitoba.ca

Received December 2005, Accepted July 2006
No. 05-CSME-66, E.I.C. Accession 2918

Abstract

The aim of this paper is to develop a complete simulation model and study the tip-over responses of mobile cranes. The developed model takes into account all factors that could affect the overturning of truck cranes including: (*i*) detailed dynamics of the manipulator links and the base that can potentially rock back and forth, (*ii*) combined vehicle suspension and ground-tire compliance, (*iii*) condition of the ground under the wheels or the outrigger pontoons, (*iv*) friction between the outriggers/tires and the ground, (*v*) spatial motion of load carried, via a rope, by the telescopic boom of the truck crane, and (*vi*) hydraulic drive system. The model also includes the effect of the presence of the wheels that can support the machine in case of ground failure at any of the outrigger pontoons, and therefore is capable of predicting subsequent responses in case of soil failure under the crane supports. Simulation results are presented to understand tip-over responses of a typical mobile crane in the presence of load lifting, load swivel, ground failure and various ground conditions. The model developed in this paper is shown to be capable of producing detailed information about the machine responses, the reaction forces at crane' supports and the state parameters of drive system to various input scenarios. The acquired information could additionally be used for improving the design of the cranes in general.

RÉPONSES DE RENVERSEMENT DES GRUES MOBILES HYDRAULIQUES

Résumé

Cet article a pour but de créer un modèle de stimulation complète et de réaliser une étude sur les réponses de renversement des grues mobiles hydrauliques. Le modèle élaboré tient compte de tous les facteurs qui pourraient toucher au renversement des grues sur camion : (*i*) dynamique détaillée des liens au manipulateur et la base qui pourrait éventuellement basculer de l'arrière à l'avant, (*ii*) la combinaison d'une suspension de véhicule et de la compliance sol-pneu, (*iii*) l'état du sol sous les roues ou les pontons du stabilisateur, (*iv*) la friction entre les stabilisateurs et les pneus et le sol, (*v*) la motion spatiale de la charge transportée, au moyen de la corde, par la flèche téléscopique de la grue sur camion, et (*vi*) le système de transmission hydraulique. Le modèle comprend également l'effet de la présence des roues qui peuvent soutenir la machine en cas d'un défaut à la terre à n'importe quel ponton de stabilisateur; il peut donc prédire des réponses subséquentes dans le cas d'une fissure du sol sous les supports de grue. Les résultats de stimulation sont présentés pour comprendre les réponses de renversement d'une grue mobile typique lors du soulèvement et du pivotement d'une charge, d'un défaut à la terre et de différents états du sol. Le modèle élaboré dans cet article offre des renseignements détaillés sur les réponses de machine, les forces de réaction aux supports de la grue et les paramètres d'état du système d'entraînement dans le cadre de différents scénarios. En outre, l'information acquise pourrait servir à améliorer la conception des grues en général.

INTRODUCTION

Tip-over stability is an important issue that should be addressed when dealing with mobile cranes. Failing to maintain stability of these machines while performing their tasks could endanger people's life and damage the machine. Although sensor systems are available for some mobile cranes to detect whether a static load exceeds the safe operating load, there is no mechanism available that includes dynamic situations. Therefore, the operator must remain alert at all times to accomplish the work efficiently and, at the same time protect his/her safety and that of others. In spite of much research in this area, the topic of mobile cranes' stability has not been fully explored and there still exist many issues that need to be further investigated. Particularly, understanding the details of the base movement during tipping over can help to define an accurate measure of stability and therefore potentially help to prevent or recover from the tipping over.

Several published articles related to the dynamics and control of mobile cranes are available in the literature. Kilicaslan et al. [1] examined the variation of the piston force with respect to the boom angular positions for different speeds of boom upward motion. The model, was used to determine the tipping loads for a planar mobile crane only and could not give information about the status of the base, i.e., whether the crane tips over completely or just rocks back and forth. Posiadala et al. [2] developed a model for analyzing load motion produced by selected controls of boom and rope in a truck crane. The truck was considered to be solidly supported by rigid base which is not realistic. Later the influence of the flexibility of the supports on the load motion was investigated by Posiadala [3]. In that work, the drive forces were presented using the so-called 'method of kinematic forcing'. Sun and Kleeberger [4] argued that 'method of kinematic forcing' does not comply with the motion during the start-up and braking. They introduced a more accurate crane model that incorporates the dynamic behavior of the hydraulic actuators to accurately describe the crane's responses to different movements of the manipulator and the load. However, modeling of tip-over stability or ground-tire interaction was not discussed in their work. Towarek [5] studied the effect of the flexible soil foundation on the dynamic stability of mobile cranes during the rotation of the boom. It was shown that considering rigid soil in the modeling phase, instead of flexible (real) soil, may result in overestimating the machine stability. Maczynski and Wojciech [6] presented a 3D model of a telescopic mobile crane. The model allowed rotation of the upper structure as well as lifting/lowering the load by means of a hoisting winch, and was used for optimization of the slewing motion of the load. Both references by Towarek [5] and, Maczynski and Wojciech [6], assumed small rotational angles of the base, and employed up-front approximation to derive the final dynamic equations. The up-front approximation approach greatly reduces the complexity of the modeling, but at the expense of developing over-simplified and sometimes questionable models. Fukagawa and Muro [7] described an alarm system to prevent overturning of truck cranes under condition of ground failure. This method, however, could deal with cases where the only destabilizing load is due to the gravitational force. In the actual case of a moving-base manipulator, a large portion of the destabilizing forces and moments could be due to the inertia arising from maneuvering the load [8]. In all the above studies, the crane's base was either considered to be fixed on the ground, or tilted by small angles. None of the pervious work, to the best of the authors' knowledge, considered the case of large rotational angles and/or translational displacement of the base. Recently, Abo-Shanab and Sepehri [9] developed a simulation model to investigate the tip-over stability of excavator machines. They also provided a detailed review of the previous work related to the general stability analysis of mobile manipulators. Mobile cranes, however, present more complicated dynamics due to the potential movements of the load. Such movements have an impact on crane stability as they increase the lever arm of the hook load and thus the destabilizing moment.

In this paper, we develop, for the first time, a comprehensive model and present simulation results, of a complete three-dimensional model for mobile cranes that are subject to tipping-over. The model includes

all factors that may affect the stability of mobile cranes: the complete rigid body dynamics of the linkage structure including the base, the flexibility of the supporting tires and/or the compliant hydraulically-actuated outriggers, bearing properties of the ground, friction properties of the contact between the supports and the ground, inertial spatial motion of load carried by a rope and, the coupled dynamic behavior of the hydraulic drive system. The model also incorporates all possible movements of the lifted load, including the effect of the load sway, which has an impact on the crane stability. Additionally, the model includes the effect of the extra support by the wheels in case of ground failure under any of the outrigger pontoons. Thus, the model is capable of predicting the crane's tip-over behavior under various scenarios including the case in which the ground is rigid or the case where the ground fails. The inclusion of all these features in one integrated model, which has not been studied in any of the previous work, is of great importance to fully understand the tip-over mechanism of mobile hydraulic cranes.

The approach taken is to first consider the connections between the base and the ground and between the end of the boom and the load as multi-degree of freedom joints. The method of virtual links [10] is then employed to reformulate the problem of modeling the non-fixed-base crane in terms of a fixed-base serial link manipulator with single degree of freedom at each joint. This process considerably simplifies the derivation of the dynamic equations by facilitating the use of formulations that already exist in many robotics textbooks. LuGre tire friction model [11] is used to determine the friction forces between the outriggers/wheels and the ground. The model is dynamic and captures most friction phenomena. The interaction between the crane and the ground is also taken into account in the development of the model. The magnitude of this interaction is the result of flexibility of the tires, compliance of the hydraulically powered outriggers, and the soil strain resulting from variable pressure of the supports and/or failure of the foundation. Kelvin-Voigt spring damping system at each outrigger and wheel is used to represent the flexibility between the outriggers/wheels and the ground [6,12]. The detailed dynamics of the hydraulic functions are fully described by a system of nonlinear differential equations describing compressibility of the hydraulic fluid, nonlinear relation between the input controls, spool displacement of the control valves and the orifice areas that control the fluid flows into and out of the respective actuators [13].

DEVELOPMENT OF THE MODEL

Modeling Multi-body System

Figure 1 shows a typical mobile boom crane. The machine consists of five parts: base, cabin, boom and telescope (which are together called telescopic boom) and the load, which is hanging by a rope via a clamming device or a hook. The base is resting on the outriggers and/or wheels, but is considered to be free to move in all directions and orientations. The cabin rotates over the base by a swing hydraulic motor through a gear train. Boom and telescope are two hydraulically-actuated links which, together with the swing motion of the cabin over the base, serve to position the end-point of the telescopic boom. The load is hanging by inextensible rope of varying length that carries the tensile force only, and has four degrees of freedom with respect to the telescopic boom: three rotations and one vertical translation. The rope passes over the telescopic boom and is connected to the main winch (hoist drum), which is fixed on the crane's cabin, and is controlled by a hydraulic motor. Therefore, the vertical movement of the load can result from the change of the telescopic boom length, its angle with respect to the cabin and, the winding (unwinding) of the rope on the hoist drum.

Figure 2 shows a top view of the machine including the wheels and the outriggers. The models of the compliance of the outriggers and the wheels, when they are in contact with the ground, are shown in Figure 3 where ${}^{W}y_{ij}(t)$ and ${}^{T}y_{ij}(t)$ denote the displacements of soil foundation under the wheels or the outriggers' pontoons due to the deformation, settlement or failure of the soil. The deformation of soil is applied to the system as a kinematic input. It is described as a function of the changing strain in time by the Duhamel integral [5], while the ground failure can be represented by Weibul distribution curve [7,

14]. During a normal operation, when the base is supported by the outriggers, the wheels are slightly above the ground and are unloaded. However, in case of soil failure under any of the outriggers' pontoons, one or more wheels come in contact with the ground, and contribute to supporting the crane.

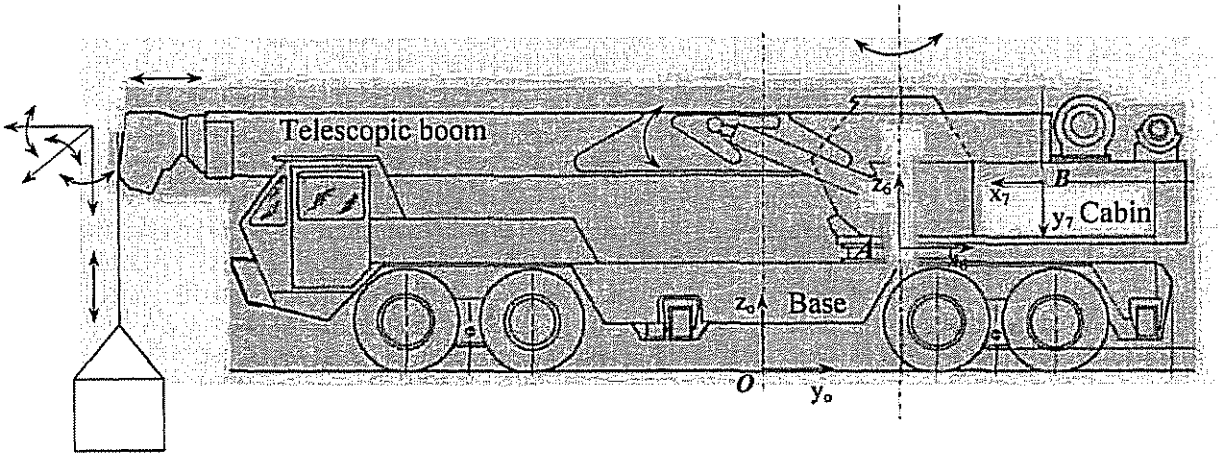

Figure 1 Typical mobile truck crane. ***O*** is the origin of the inertial coordinate frame, ***A*** is the origin of the base coordinate frame, and ***B*** is the origin of the coordinate frame attached to the cabin (original picture was taken from a P&H-T250 operator manual).

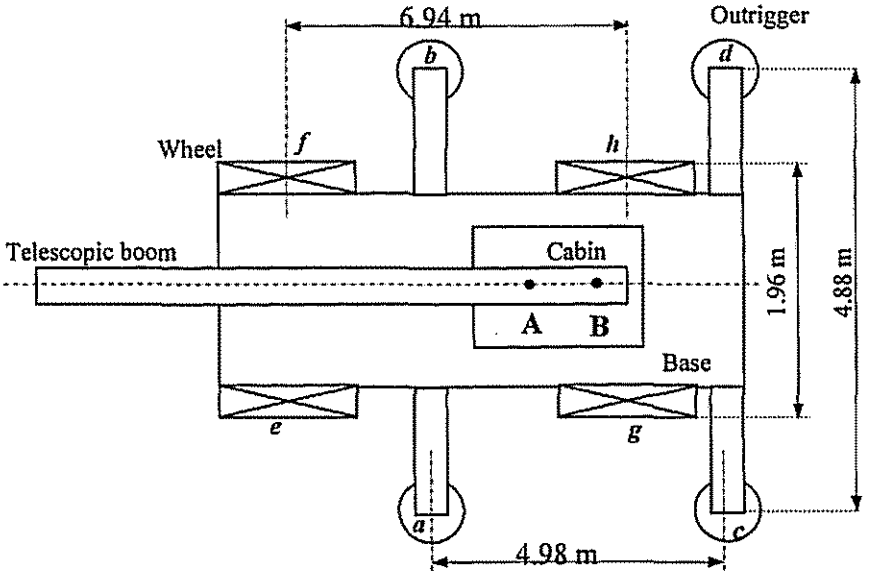

Figure 2 Schematic top view of crane.

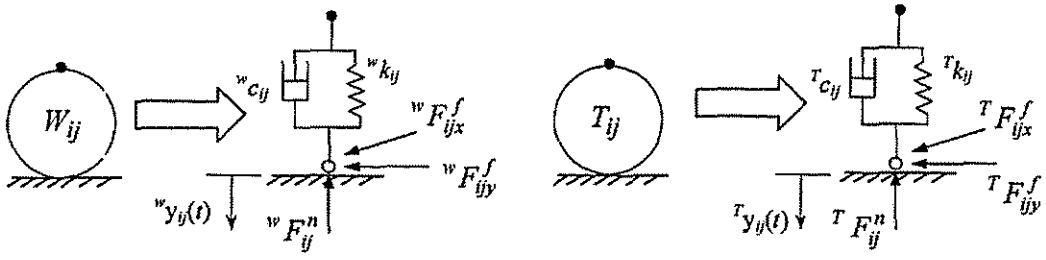

Figure 3 Models of compliance of the wheels and the outriggers when they are in contact with the ground that could deform or fail.

To describe the motion of the base, five virtual serial links are added between the ground and the base. This allows the base to be considered as the last link of a six degree-of-freedom serial link manipulator. The configuration of the manipulator is *PPPRRR*, i.e., the first three links have prismatic (*P*) joints and the last three links are connected together by revolute (*R*) joints (see Figure 4). Furthermore, three virtual links are added between the end-point of the telescopic boom and the load, allowing the motion of the load, with respect to the end of the boom, be described by a four degree-of-freedom serial link manipulator with *RRRP* kinematic configuration. The addition of these eight virtual links will allow the entire crane that contains a load with multiple-degree-of-freedom joint and a non-fixed base to be transferred into a thirteen degree-of-freedom fixed base serial-link manipulator with single-degree-of-freedom joints. This process allows the use of existing formulations, documented in robotics textbooks, to derive the corresponding dynamic equations. Once, the equations of motion, describing the expanded system are derived, the final equations of motion for the original five-link system are obtained by setting all the kinematic and dynamic parameters pertaining to the virtual links to zero (see reference [10] for detailed description of the method and examples).

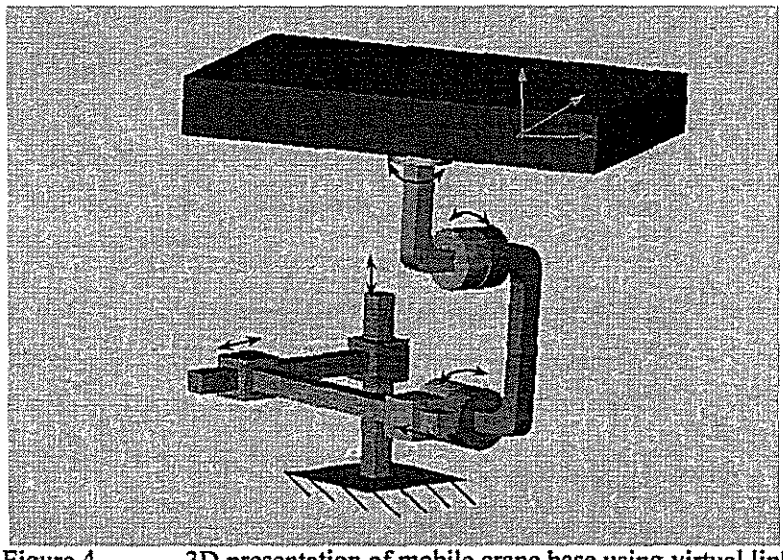

Figure 4 3D presentation of mobile crane base using virtual links.

The Denavit-Hartenberg coordinate systems pertaining to the machine kinematics are shown in Figure 5 and the kinematic parameters are given in Table 1. The final dynamic equations can be written in the following general form:

$$\tau = \mathbf{M}(\mathbf{q})\ddot{\mathbf{q}} + \mathbf{C}(\mathbf{q},\dot{\mathbf{q}}) + \mathbf{G}(\mathbf{q}) + \mathbf{J}^{\mathrm{T}}\mathbf{F} \qquad (1)$$

where $\mathbf{M}(\mathbf{q})$ is the symmetric, positive definite inertial acceleration-related matrix, $\mathbf{C}(\mathbf{q},\dot{\mathbf{q}})$ is the vector of centripetal and Coriolis torques and, $\mathbf{G}(\mathbf{q})$ is the vector of gravitational torques, which also includes the effect of the inclination of the whole machine. $\mathbf{q} = \{q_1, q_2, ..., q_{13}\}^T$, $\dot{\mathbf{q}}$ and $\ddot{\mathbf{q}}$ are vectors of the joint variables, velocities and accelerations, $\tau(t) = \{\tau_1, \tau_2, .., \tau_{13}\}^T$ is the vector of the generalized force applied at the corresponding joints. The term $\mathbf{J}^{\mathrm{T}}\mathbf{F}$ reflects the effect of the external forces, due to the interaction between the crane supports and the ground, at the manipulator joints. $\mathbf{F}$ is the force/torque vector representing the summation of all external forces transferred to point A on the base (the origin of the coordinate frame 6, as shown in Figures 1, 2, and 5). $\mathbf{J}$ is the Jacobian matrix used to calculate the effect of $\mathbf{F}$ on each joint.

Table 1 Kinematic parameters of the machine under investigation.

Link	q_i (rad)	d_i (m)	a_i(m)	α_i (rad)
1	$\pi/2$	q_1	0	$\pi/2$
2	$\pi/2$	q_2	0	$\pi/2$
3	0	q_3	0	0
4	q_4	0	0	$-\pi/2$
5	q_5	0	0	$-\pi/2$
6	q_6	0.66	1.0	0
7	q_7	0.85	-1.51	$-\pi/2$
8	q_8	0	0	$-\pi/2$
9	π	q_9	0	0
10	q_{10}	0	0	$-\pi/2$
11	q_{11}	0	0	$\pi/2$
12	q_{12}	0	0	0
13	0	q_{13}	0	0

The normal force vector at each outrigger, ${}^{T}\mathbf{F}^{n} = \{{}^{T}F_{fr}^{n}, {}^{T}F_{fl}^{n}, {}^{T}F_{rr}^{n}, {}^{T}F_{rl}^{n}\}^{\mathrm{T}}$, or each wheel, ${}^{W}\mathbf{F}^{n} = \{{}^{W}F_{fr}^{n}, {}^{W}F_{fl}^{n}, {}^{W}F_{rr}^{n}, {}^{W}F_{rl}^{n}\}^{\mathrm{T}}$, are calculated based on the deflection of the spring damper system. For example, the normal force component at the front right outrigger, ${}^{T}F_{fr}^{n}$, is calculated as follows:

$$ {}^{T}F_{fr}^{n} = \frac{\partial {}^{T}R_{fr}}{\partial \dot{q}_1} + \frac{\partial {}^{T}V_{fr}}{\partial q_1} \tag{2} $$

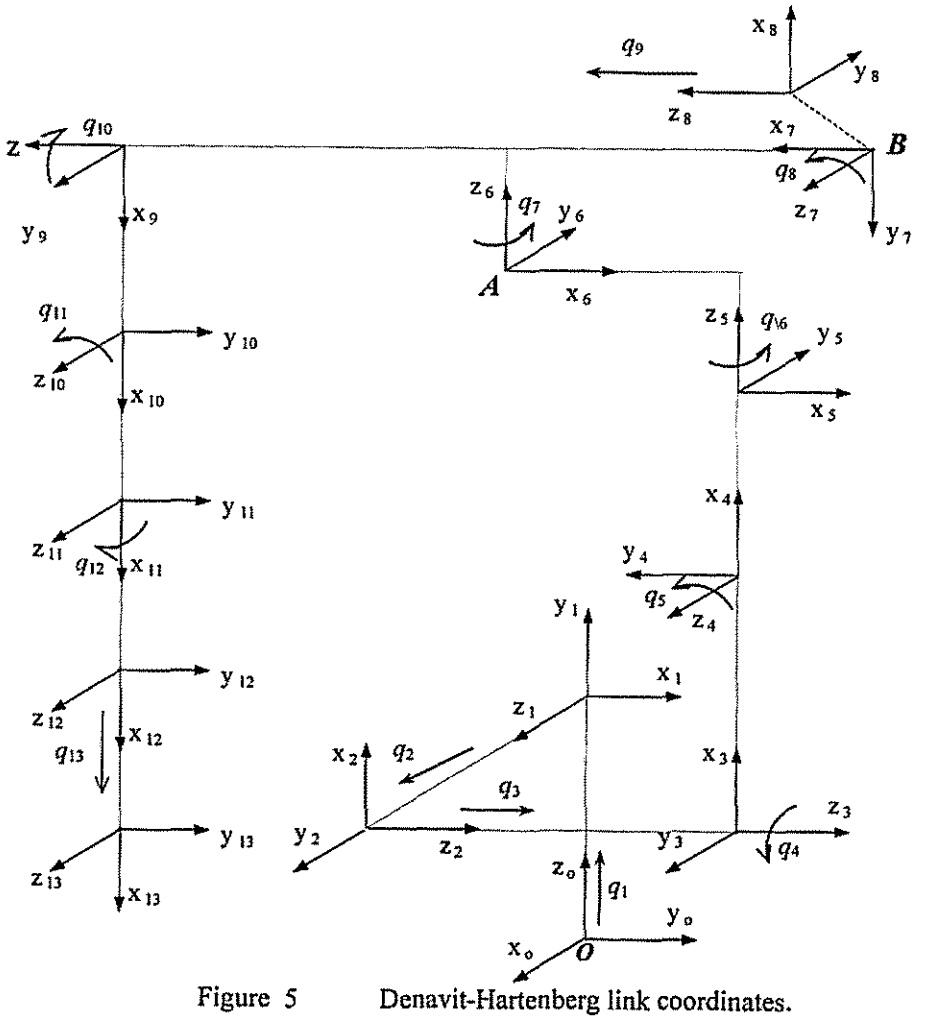

Figure 5 Denavit-Hartenberg link coordinates.

where R denotes the Rayleigh's dissipation function and V is the potential energy function due to the spring.

$$ {}^{T}R_{fr} = \frac{1}{2} {}^{T}c_{fr} \left[\frac{d}{dt} \left\{ \mathbf{T}_6 \, {}^{T}\mathbf{r}_{fr}^{6} \right\}_z - {}^{T}\dot{y}_{fr}(t) \right]^2 \tag{3} $$

$$ {}^{T}V_{fr} = \frac{1}{2} {}^{T}k_{fr} \left[\left\{ \mathbf{T}_6 \, {}^{T}\mathbf{r}_{fr}^{6} \right\}_z - {}^{T}y_{fr}(t) \right]^2 \tag{4} $$

Thus,

$$ {}^{T}F_{fr}^{n} = \left({}^{T}c_{fr} \left[\left\{ \left[\sum_{i=1}^{6} \frac{\partial \mathbf{T}_6}{\partial q_i} \dot{q}_i \right] {}^{T}\mathbf{r}_{fr}^{6} \right\}_z - {}^{T}\dot{y}_{fr}(t) \right] + {}^{T}k_{fr} \left[\left\{ \mathbf{T}_6 \, {}^{T}\mathbf{r}_{fr}^{6} \right\}_z - {}^{T}y_{fr}(t) \right] \right) \left\{ \frac{\partial \mathbf{T}_6}{\partial q_1} {}^{T}\mathbf{r}_{fr}^{6} \right\}_z \tag{5} $$

where , ${}^{T}r_{fr}^{6}$ is the position vector of front right outrigger defined in coordinate frame 6 (see Figure 5). c and k denote the damping and stiffness coefficients, respectively. The subscript z means the z component of the vector and, $\mathbf{T}_6$ is the homogeneous transformation matrix from coordinate frame 6 to the reference (base) coordinate frame o.

LuGre tire friction model [11] is used to calculate the friction forces between the outriggers and the ground. This dynamic model can describe steady-state friction characteristics and supports hysteresis behavior due to frictional lag and spring-like behavior in stiction. It also produces a varying breakaway force depending upon the rate of changing the applied force. Using LuGre model, the x component of the friction force at the front right outrigger, i.e., ${}^{T}F_{frx}^{f}$, is determined as:

$$ {}^{T}F_{frx}^{f} = \left({}^{T}\sigma_{o\,frx}\,{}^{T}z_{frx} + {}^{T}\sigma_{1\,frx}\,{}^{T}\dot{z}_{frx} + {}^{T}\sigma_{2\,frx}\,{}^{T}v_{frx} \right) {}^{T}F_{fr}^{n} \tag{6} $$

where σ_o is the normalized lumped stiffness, σ_1 the normalized lumped damping, σ_2 is the normalized viscous relative damping, F^n represents the normal force. The average deflection of the bristles at the front right outrigger in x direction, ${}^{T}z_{frx}$, is modeled as

$$ {}^{T}\dot{z}_{frx} = {}^{T}v_{frx} - \frac{{}^{T}\sigma_{o\,frx}\left|{}^{T}v_{frx}\right|}{{}^{T}\eta_x({}^{T}v_{frx})}\,{}^{T}z_{frx} \tag{7} $$

where v denotes the relative velocity between the outrigger and the ground. Function $\eta(v)$ contains information about the velocity dependence of friction. It is positive and depends on many factors such as material properties, lubrication, and temperature.

$$ {}^{T}\eta_x({}^{T}v_{frx}) = {}^{T}\mu_{c\,frx} + ({}^{T}\mu_{s\,frx} - {}^{T}\mu_{c\,frx})\, e^{-\left|\frac{{}^{T}v_{frx}}{{}^{T}v_{s\,frx}}\right|^{0.5}} \tag{8} $$

In (8) μ_c is the Coulomb friction coefficient and μ_s is the static friction coefficient. v_s is the Stribeck velocity, which helps to define the velocity dependence of friction.

Modeling Hydraulic Drive System

Figure 6 shows a schematic diagram of typical hydraulic power circuit adopted in this paper. The power required to actuate the hydraulic cylinders and the hydraulic motors is supplied by the engine, which drives four hydraulic pumps through a gear train. The output of each pump is used to operate a separate hydraulic actuator by an open-center valve as shown in the figure. Figure 7 shows the operation of the open-center valve in actuating the hydraulic cylinder. When the spool of the open-center valve is in neutral position, the flow passes through the valve and returns to the tank. As the spool moves to the left or to the right, the flow is distributed to the load and the tank, depending upon the orifice arrangement and the load. A diesel engine is used to turn the four axial-piston variable-displacement pumps. The angles of the swash plates, for all four pumps, are equally controlled according to the summing pressure, $P_1 + P_2 + P_3 + P_4$. Consequently, these pumps have identical output flow, but could operate at different output pressures.

With reference to Figure 8, the output pump pressures are applied to four small pistons (two are shown in Figure 8) that change the angle of the swash plate against three parallel springs. This mechanical feedback system serves to limit the power that is drawn from the engine, so that the pressure-flow curve is below the power limit curve as shown in Figure 8.

Assuming that the losses due to leakage are negligible, the equations governing the flow distribution, for each actuator, can be written as follows [13]:

$$Q_i = ka_i\sqrt{P_s - P_i} \tag{9}$$

$$Q_o = ka_o\sqrt{P_o - P_e} \tag{10}$$

$$Q_e = Q - Q_i = ka_e\sqrt{P_s - P_e} \tag{11}$$

where Q_i , Q_o, and Q_e are the inlet, outlet, and exit flows, to and from the cylinder, respectively. Q is the supply flow. a_i, a_o and a_e are the inlet, outlet and exit areas, respectively (see Figure 7). k is the orifice coefficient. The rate of change of the inlet pressure $\dot{P}_i$ and the outlet pressure $\dot{P}_o$, for each actuator, are:

$$\dot{P}_i = \frac{\beta}{V_i(X)}\left(Q_i - A_i\dot{X}\right) \tag{12}$$

$$\dot{P}_o = \frac{\beta}{V_o(X)}\left(A_o\dot{X} - Q_o\right) \tag{13}$$

where X denotes actuator displacement, $\dot{X}$ is the actuator velocity and β is the effective bulk modulus. A_i and A_o are the effective piston areas.

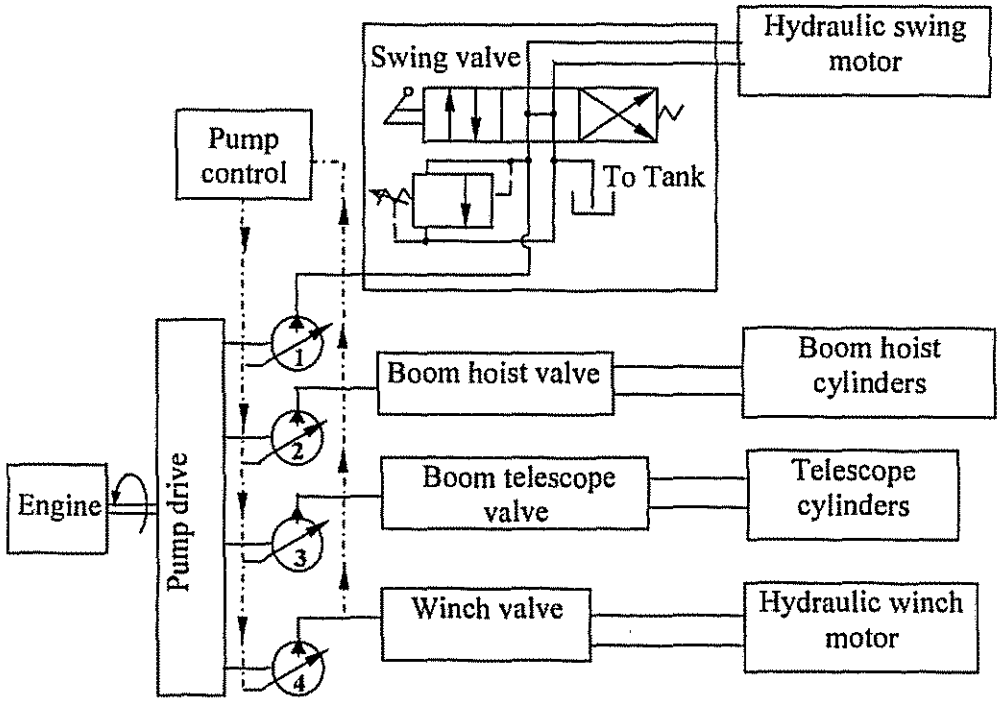

Figure 6 Schematic diagram of typical hydraulic power circuit. Parts labeled 1, 2, 3, and 4 are the hydraulic pumps. Boom hoist valve, boom telescope valve and winch valve are similar to the swing valve, which is shown in detail.

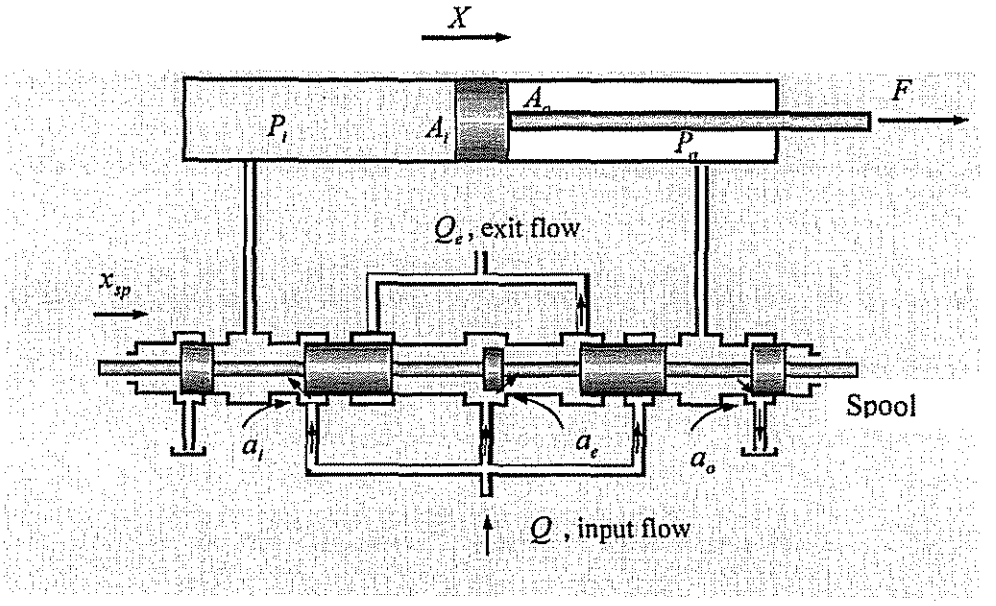

Figure 7 Typical hydraulic cylinder actuated by an open-center valve.

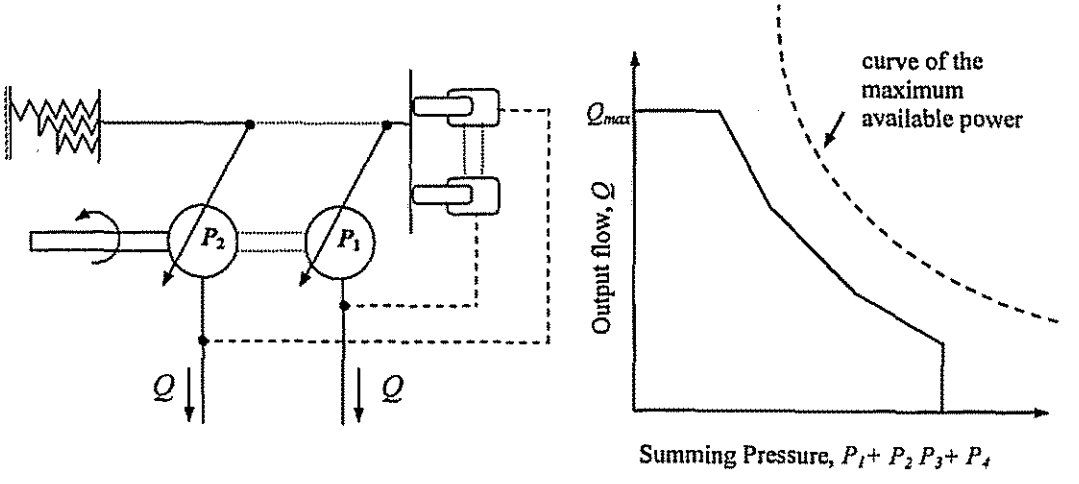

Figure 8 Relation between the summing pressure and the pump output flows for the variable displacement pumps used in boom crane.

$V_i(X)$ and $V_o(X)$ are the volumes of the fluid trapped at the sides of the actuator. They are expressed as

$$V_i(X) = \overline{V}_i + X A_i \tag{14}$$

$$V_o(X) = \overline{V}_o - X A_o \tag{15}$$

$\overline{V}_i$ and $\overline{V}_o$ are the volumes of fluid trapped initially at either sides of the actuator. The output force from each actuator, F, is

$$F = P_i A_i - P_o A_o \tag{16}$$

Finally, the torque generated by the hydraulic cylinder is:

$$\tau = F \frac{dX}{d\theta} \tag{17}$$

where $\frac{dX}{d\theta}$ represents the nonlinear relationship between the actuator linear velocity, $\dot{X}$, and the corresponding link rotational velocity, $\dot{\theta}$. For the swing and winch hydraulic motors, equations (12), (13) and (17) must be written in the following forms:

$$\dot{P}_i = \frac{\beta}{V_i(X)}\left(Q_i - D_m \dot{X}\right) \tag{18}$$

$$\dot{P}_o = \frac{\beta}{V_o(X)}\left(D_m \dot{X} - Q_o\right) \tag{19}$$

$$\tau = n D_m (P_i - P_o) \tag{20}$$

where D_m is the volumetric displacement of the motor, and n is the gear reduction from the hydraulic motor to the output shaft. The relationship between the spool displacement, x_{sp}, and the input voltage, u, to the servovalve can be adequately expressed by a first-order differential equation:

$$u = \left(\frac{\tau_c}{k_{sp}}\right)\frac{dx_{sp}}{dt} + \left(\frac{1}{k_{sp}}\right)x_{sp} \tag{21}$$

where τ_c and k_{sp} are gains describing the valve dynamics.

SIMULATION STUDIES

Having determined, the comprehensive equations describing the model of the entire crane, in this section, we present a number of case studies illustrating tip-over responses under various motion controls and soil conditions that influence the overturning of the cranes. For simulations, the values of dynamic parameters corresponding to the adopted model of the machine under investigation are listed in Table 2. The stiffness and damping coefficient values of the wheel-tire compliance were chosen as: ${}^{w}k_{fr} = {}^{w}k_{fl} = {}^{w}k_{rr} = {}^{w}k_{rl} = 17.5\times10^{5}$ N/m and ${}^{w}c_{fr} = {}^{w}c_{fl} = {}^{w}c_{rr} = {}^{w}c_{rl} = 7.5\times10^{4}$ Ns/m. These values provide a natural frequency of ≈ 3 Hz and a damping ratio of ≈ 0.4 in the vertical direction for the vehicle with no load. Note that the natural frequencies and damping ratios change with the manipulator configuration and payload. The stiffness and damping coefficient of the compliance between the outriggers and the ground were chosen as ${}^{T}k_{fr} = {}^{T}k_{fl} = {}^{T}k_{rr} = {}^{T}k_{rl} = 20\times10^{6}$ N/m and ${}^{T}c_{fr} = {}^{T}c_{fl} = {}^{T}c_{rr} = {}^{T}c_{rl} = 2.55\times10^{6}$ Ns/m. The coefficients of the friction between the wheels and the ground were chosen as ${}^{w}\mu_{s_{fr}} = {}^{w}\mu_{s_{fl}} = {}^{w}\mu_{s_{rr}} = {}^{w}\mu_{s_{rl}} = 0.9$ and ${}^{w}\mu_{c_{fr}} = {}^{w}\mu_{c_{fl}} = {}^{w}\mu_{c_{rr}} = {}^{w}\mu_{c_{rl}} = 0.7$. The values of other parameters used in LuGre model are given below:

${}^{w}\sigma_{o_{fr}} = {}^{w}\sigma_{o_{fl}} = {}^{w}\sigma_{o_{rr}} = {}^{w}\sigma_{o_{rl}} = 401/\text{m}$, ${}^{w}\sigma_{1_{fr}} = {}^{w}\sigma_{1_{fl}} = {}^{w}\sigma_{1_{rr}} = {}^{w}\sigma_{1_{rl}} = 4.9487$ s/m,

${}^{w}\sigma_{2_{fr}} = {}^{w}\sigma_{2_{fl}} = {}^{w}\sigma_{2_{rr}} = {}^{w}\sigma_{2_{rl}} = 0.0018$ s/m, and ${}^{w}v_{s_{fr}} = {}^{w}v_{s_{fl}} = {}^{w}v_{s_{rr}} = {}^{w}v_{s_{rl}} = 12.5$ m/s.

The above values were used by Canudas de Wit and Tsiotras [11] for tire friction models and gave results that matched reasonably well with their experimental data and are therefore adopted here.

Table 2 Masses and coordinates of center of gravities in local coordinate frames.

	mass (kg)	x_c (m)	Y_c (m)	z_c (m)
Base	12,000	-1.8	0.0	-0.33
Cabin	4,000	0.0	0.26	0.0
Boom	2,400	0.3	0.0	2.83
Telescope	1,600	0.35	0.0	-4.5
Clamming Device	790	0.0	0.0	0.0

Case Study 1: Effect of Ground Failure at One Support

In this study, we consider a case where the clamming device is holding a load of 5000kg and the boom reach is 14m. The machine is initially resting on rigid ground by four outriggers (see Figure 9). We then simulate tip-over of the crane in case of ground failure under the front left outrigger pontoon (marked 'a' in Figure 9) at $t \approx 4$s. Figure 10 illustrates the course of changes of Euler angles (q_4, q_5 and q_6 in Figure 5) that describe the orientation of the base coordinate frame $\{x_6y_6z_6\}$ with respect to the inertial frame $\{x_oy_oz_o\}$, during two possible scenarios. In the first scenario, no action is taken and the crane is completely over-turned. In the second scenario, the load is dropped (at $t\approx7$s) when the base tips more than 15°. As is seen in Figure 10, in the second scenario, the crane rolls back and regains stability. Figure 11 shows the noticeable swaying of the clamming device around the end-point of the telescopic boom in the second scenario. The changes of two main rotations (i.e., coordinates, q_{10} and q_{11} in Figure 5) are shown in the figure. Figure 12 shows the reaction forces at four outriggers as well as the front wheels during the crane motion. As is seen, there are no reaction forces at the front wheels and the rear right outrigger before the ground failure. Thus, the support polygon for the crane before the ground failure is ***abca*** (refer to Figure 9). After the ground failure occurs under the outrigger pontoon 'a', the front left and the front right wheels come in contact with the ground in supporting the crane. For a short period of time, the support polygon becomes ***efce***. Then the crane starts to tip over around the edge ***ec***; this is clearly seen from Figure 12, as the supports at the front and the rear right outriggers as well as the front right wheel break free of the soil. Finally, after the crane regains stability, the support polygon becomes ***efbce***.

Case Study 2: Effect of Lifting/Lowering the Load

In this case study, the effect of a load lowering/lifting action on crane tip-over responses is investigated. The crane is initially resting on the outriggers and holding a 3500kg load at a boom angle of $\approx 55^{\circ}$. It then lowers the load to $\approx 31^{\circ}$ (see Figure 13) at which the crane starts to tip over. At this moment we consider two different scenarios. In the first scenario, as soon as the crane starts to tip over, the operator moves the boom up in anticipation that this reverse motion will bring the machine back to a stable situation. In the second scenario, the operator stops the boom immediately and no further action is taken. With reference to Figure 13, it is seen that the machine tilts about 5.5° in the first scenario whereas it tilts less than 4° in the second scenario. It is therefore concluded that in this case study, the dynamic reaction forces as a result of the reversal motion of the boom, would promote instability. Thus, taking no action by the operator would produce a safer tip-over response. This case study also reveals the importance of tip-over simulation studies in understanding the mechanism of tip-over and potentially developing means to prevent tip-over situations.

Case Study 3: Effect of Swing Motion

In this example, the crane is resting on the outriggers with the clamming device holding a 3500kg load. The task is to rotate the entire upper structure about 360° at two different speeds: 27 deg/s and 18 deg/s. With reference to Figure 14, when the machine rotates at 27 deg/s, it rocks approximately 1° around the '*ac*' axis and about 2° around the '*cd*' axis. When rotating at the lower speed of 18 deg/s, it hardly lifts up about these axes. Figure 15 shows that unfavorable oscillations of the load, hanging by the rope, during the swing motion. The projection of the motion trajectory on the horizontal plane perpendicular to the axis of swing rotation is also shown in Figure 15.

Case Study 4: Effect of Friction Between the Wheels and the Ground

The sensitivity of the machine stability to various friction conditions between the wheels and the ground is investigated in this case study. The crane is initially resting on its wheels and the clamming device is holding a 1000kg load with the boom reaching a 12m length. The load then swings for approximately 180°. Different values for friction coefficients between the wheels and the ground are applied for this motion: high friction ($\mu_s = 0.9$ and $\mu_c = 0.7$), medium friction ($\mu_s = 0.1$ and $\mu_c = 0.06$), and low friction ($\mu_s = 0.08$ and $\mu_c = 0.03$). Figure 16 shows the swivel motion of the load and the base movement. As is seen, the base rotational angles q_4 and q_5 (the latter not shown for the sake of brevity) are almost the same given all three friction conditions. However, the less the friction between the wheels and the ground, the more the machine skids around the vertical axis, and the operator may lose control of the machine which is dangerous and should be avoided.

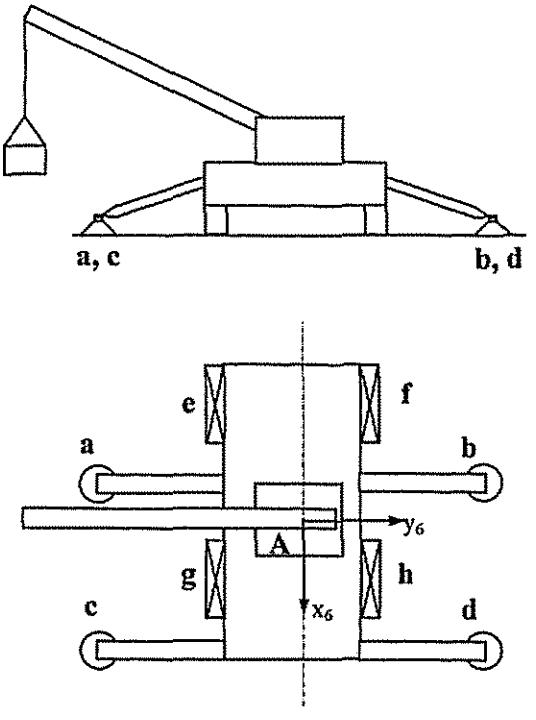

Figure 9 Mobile crane configuration in Case study 1.

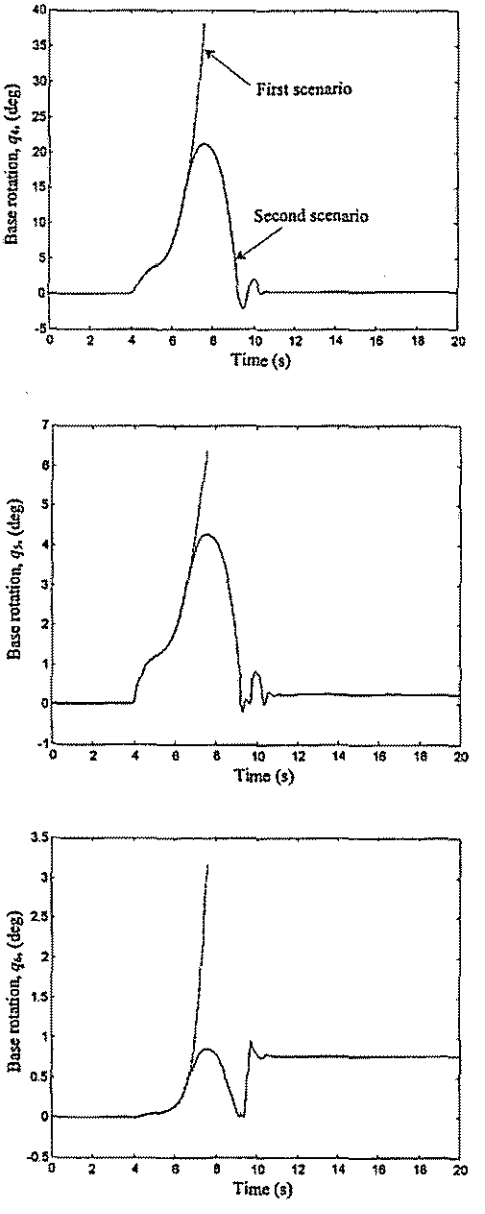

Figure 10 Trajectories of Euler angles describing spatial base rotation with respect to the inertial frame (Case study 1; two scenarios).

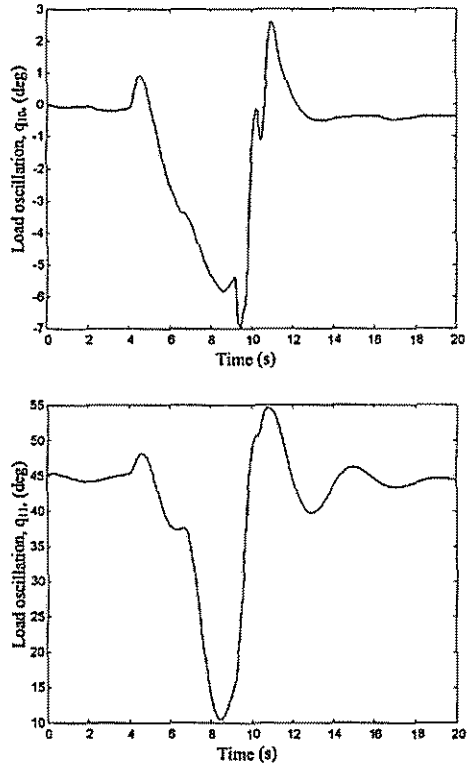

Figure 11 Swaying of the clamming device (Case study 1; second scenario).

CONCLUDING REMARKS

In this paper, a complete highly nonlinear and coupled model of the dynamics of mobile hydraulic cranes was developed for the purpose of simulating and studying the overturning behavior of these machines. The model takes into account (*i*) the hydraulic actuation functions, (*ii*) the detailed dynamics of the manipulator base that can rock back and forth, (*iii*) the flexibility and friction of the contact between the crane supports and the ground, (*iv*) the effect of swaying of the load carried by a rope and (*v*), the condition of ground failure at any of the crane supports. As a result, a most exact representation, to the best of our knowledge, of the dynamic behavior of hydraulic cranes carrying a load by a rope was developed. Using the model, a simulation program was constructed to study various dynamic stability scenarios that: (*i*) could be dangerous to perform on the actual system, and (*ii*) were not possible by models developed prior to this work. In particular, simulations were conducted to study tip-over responses in the presence of load lifting, load swivel, ground failure and various ground conditions. It was discussed that proper manipulation of the telescopic boom can prevent certain tip-over situations resulting from ground failure under any of the crane outriggers. Simulation results also revealed that no straightforward correlation exists between the frictional properties of the base and the ground, and the machine stability. However, reducing the friction leads to skidding of the whole machine and loss of control of the crane. These results could be used to improve the operations and even the design of truck cranes.

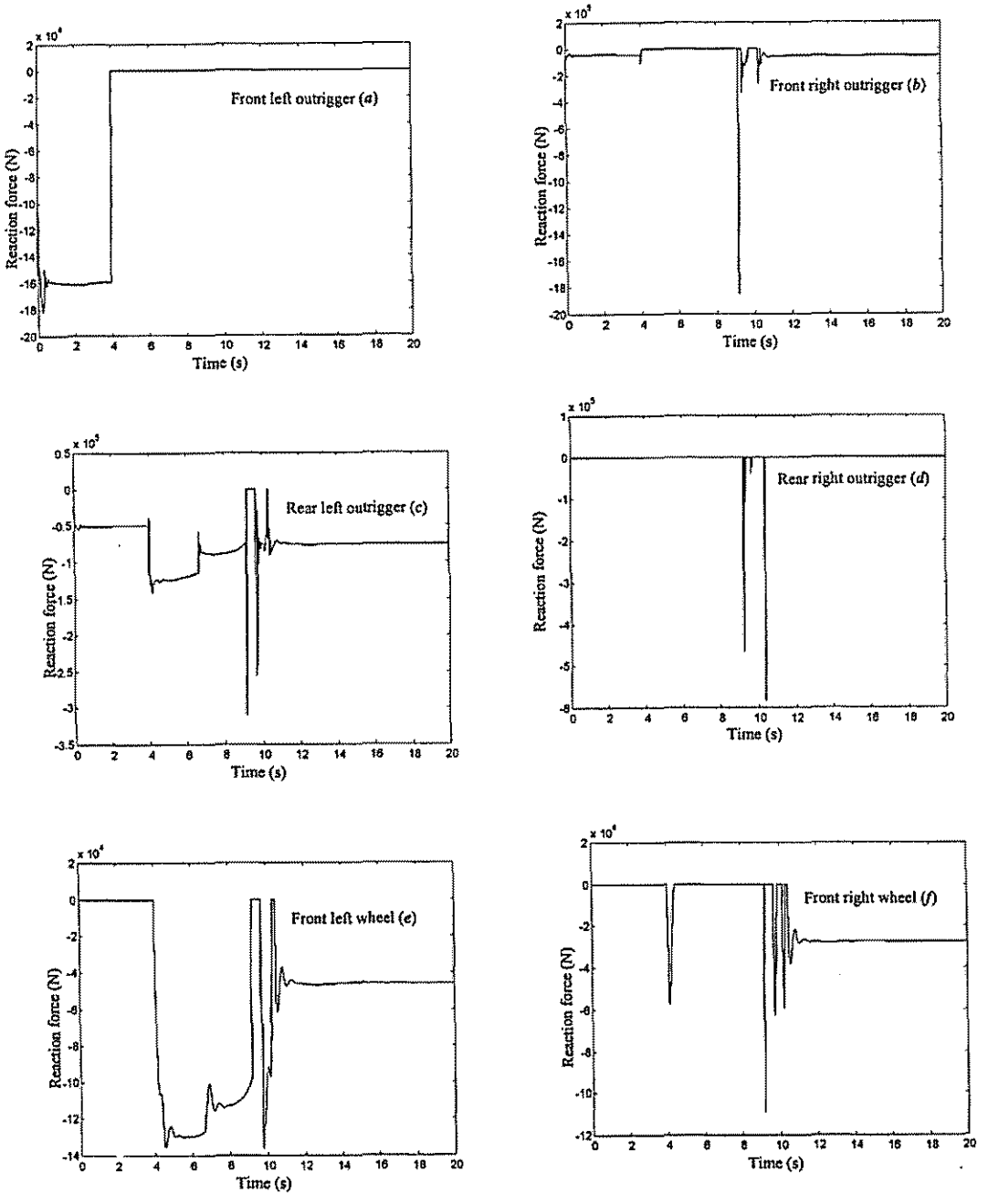

Figure 12 Reaction forces at crane supports (Case study 1; second scenario).

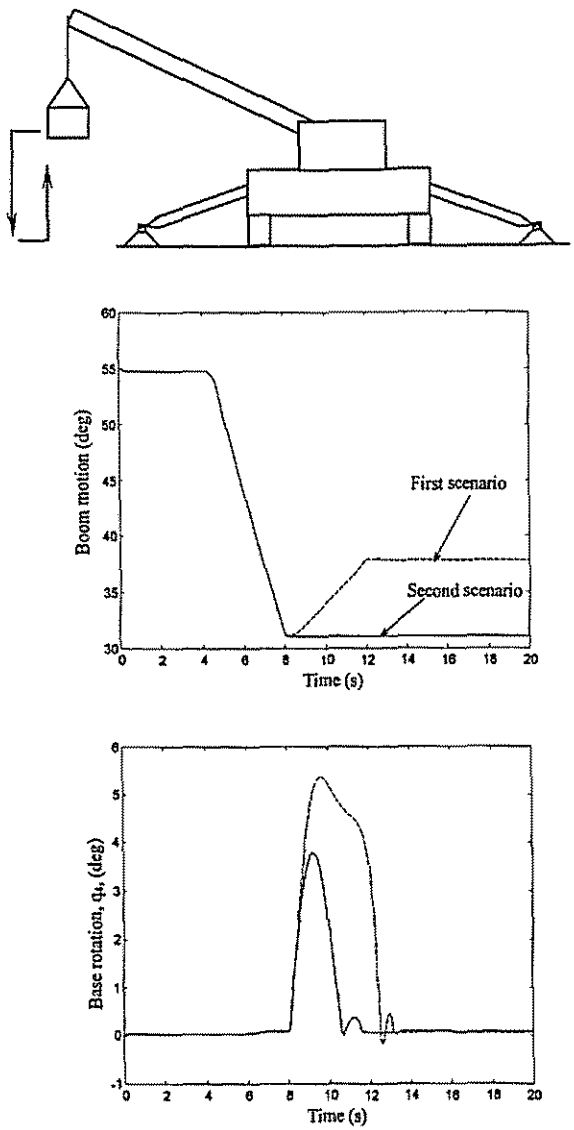

Figure 13 Effect of boom motion on base stability (Case study 2).

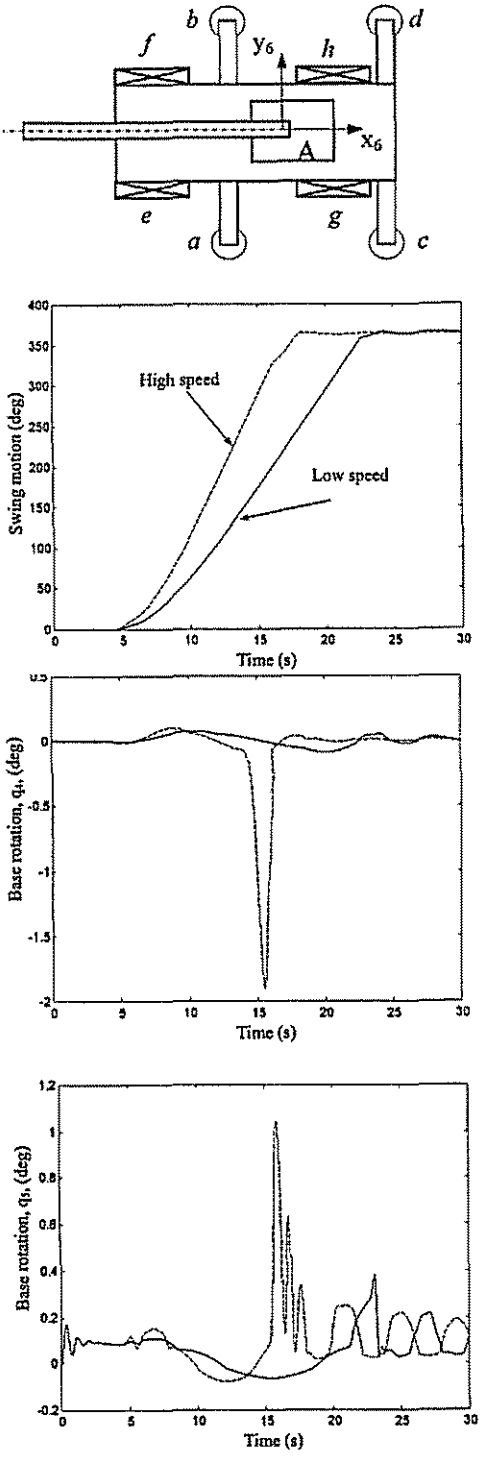

Figure 14 Mobile crane states during swivel of load hanging by rope (Case study 3).

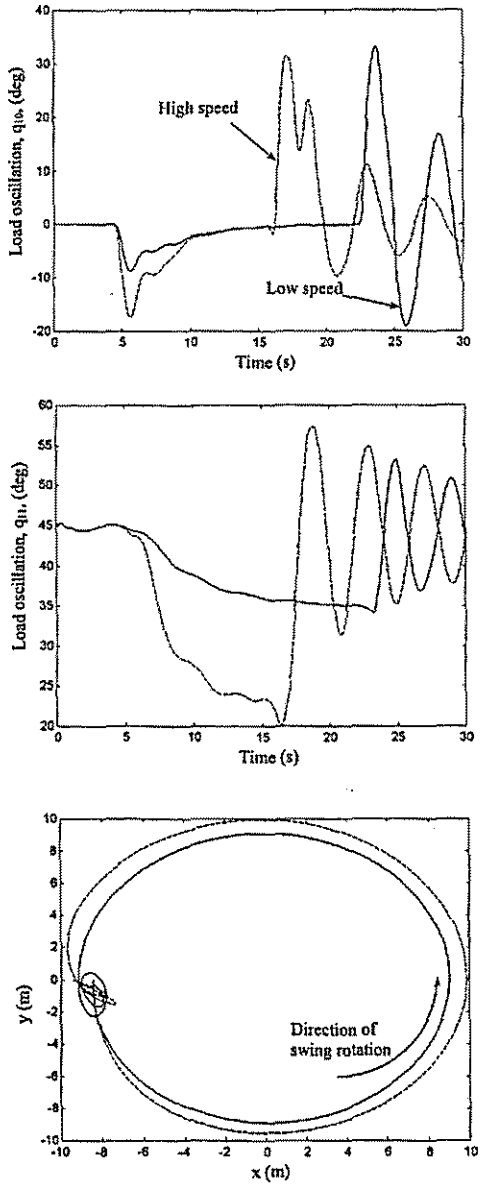

Figure 15 Load oscillations and projection on horizontal plane (Case study 3).

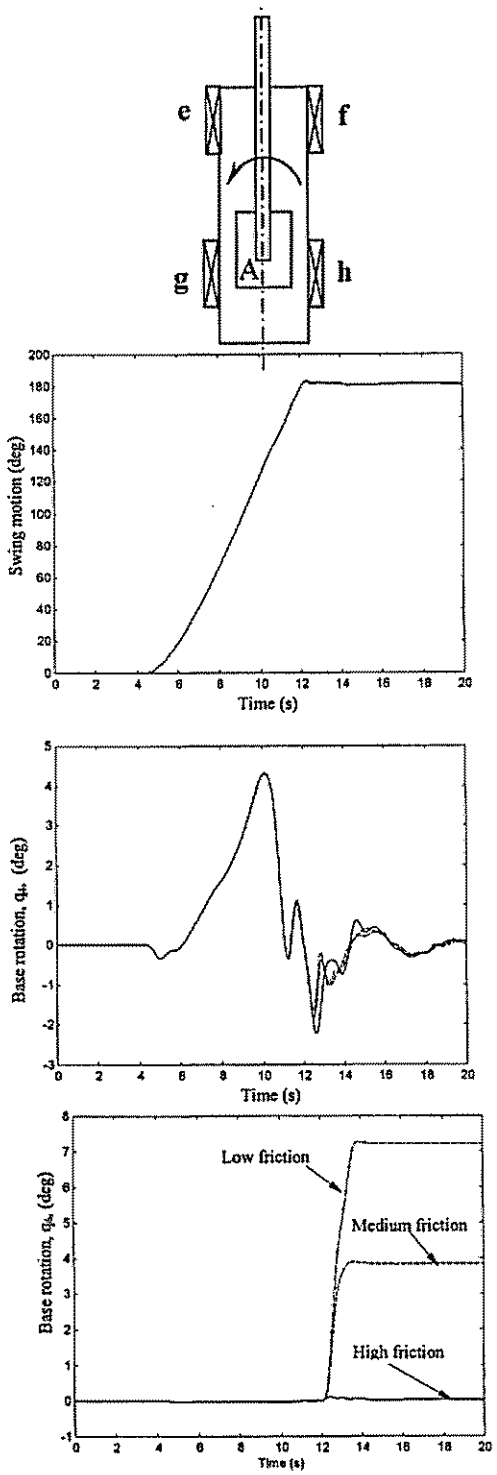

Figure 16 Effect of friction on stability (Case study 4).

REFERENCES

[1] S. Kilicaslan, T. Balkan, and S.K. Ider, "Tipping loads of mobile cranes with flexible booms," *Journal of Sound and Vibration* **223**, 645-657, 1999.

[2] B. Posiadala, B. Skalmierski, and L. Toski, "Motion of the lifted load brought by a kinematic forcing of the crane telescopic boom," Mechanism and Machine Theory **25**, 547-556, 1990.

[3] B. Posiadala "Influence of crane support system on motion of lifted load," *Mechanism and Machine Theory* **32**, 9-20, 1997.

[4] G. Sun and M. Kleeberger, "Dynamic responses of hydraulic mobile crane with consideration of the drive system," *Mechanism and Machine Theory* **38**, 1489-1508, 2003.

[5] Z. Towarek, "The Dynamic stability of a crane standing on soil during the rotation of the boom," *International Journal of Mechanical Science* **40**, 557-574, 1998.

[6] A. Maczynski and S. Wojciech, "Dynamic of a mobile crane and optimization of the slewing motion of its upper structure," *Nonlinear Dynamics* **32**, 259-290, 2003

[7] Fukagawa and T. Muro, "Alarm system to prevent the overturning of truck cranes considering possible ground failure," *Proceedings of the 11th International Symposium on Automation and Robotics in Construction,* Brighton, UK, 27-34, 1994.

[8] A. Ghasempoor and N. Sepehri, "A Measure of Stability for Mobile Manipulators With Application to Heavy Duty Hydraulic Machines," *ASME Journal of Dynamic Systems, Measurement, and Control* **120**, 360-370, 1998

[9] R.F. Abo-Shanab and N. Sepehri, "Tip-over Stability of Manipulator-Like Mobile Hydraulic Machines," *ASME Journal of Dynamic Systems, Measurement, and Control* **127**, 295-301, 2005.

[10] R.F. Abo-Shanab, N. Sepehri, and Q. Wu, "On Dynamic Modelling of Robot Manipulators: The Method of Virtual Links," Proceedings *ASME Design Engineering Technical Conference*, Montreal, Canada, Paper #DETC02/MECH-34225, 2002.

[11] C.C. de Wit and P. Tsiotras, "Dynamic Tire Friction Models for Vehicle Traction Control," Proc. 38th Conf. on Decision and Control, Phoenix, AZ, 3746-3751, 1999.

[12] U.O. Akpan and M. R. Kujath, "Sensitivity of a Mobile Manipulator Response to System Parameters," *ASME Journal of Vibration and Acoustics* **120**, 156-163, 1998.

[13] Merritt, H.E., *Hydraulic Control Systems*, John Wiley and Sons, NY, 1967.

[14] K. Uto, M. Fuyuki and M. Sakurai, "An exponential mathematical model to geotechnical curves", *Proc. Int. Symp. on Penetrability and Drivability of Piles*, 1985.

NOMENCLATURE

$\mathbf{q}, \dot{\mathbf{q}}, \ddot{\mathbf{q}}$	vectors of the joint angles, velocities and accelerations, respectively
$\mathbf{T}_i$	homogeneous transformation matrix from frame *i* to reference frame
$\mathbf{z}_i$	*z-axis* of coordinate frame *i*
$\mathbf{p}_i$	position vector of the origin of coordinate frame *i*
$\mathbf{I}_i^i$	inertial matrix of link *i* about its mass center in coordinate frame *i*
$\mathbf{r}_i^i$	position vector of mass center of link *i* in coordinate frame *i*
$\mathbf{g}$	gravitational acceleration vector in base coordinate frame
$\mathbf{J}$	Jacobian matrix
$\mathbf{F}, \tau$	vectors of force and generalized force/torque, respectively
$\mathbf{M}$	inertial matrix
$\mathbf{C}, \mathbf{G}$	centripetal and Coriolis torques vector, vector of gravitational torques
a_i, a_o, a_e	inlet, outlet and exit orifice areas, respectively
P_i, P_o	line pressures
P_s, P_e	supply and tank pressures, respectively
Q_i, Q_o, Q_e	flow into valve, out of valve and from pump to tank, respectively
X	actuator linear displacement.
β	effective bulk modulus of the drive system
m_i	mass of link *i*
k	stiffness coefficient
C	damping coefficient
A	piston area
D_m	volumetric displacement of the hydraulic motor
x_{sp}	valve spool displacement
μ_s	static (stick) friction coefficient
μ_c	coulomb (slip) friction coefficient
$\sigma_o, \sigma_1, \sigma_2$	normalized lumped stiffness, damping and viscous relative damping, respectively
z	bristle deflection
Superscripts	
n	normal force
f	friction force
T	outrigger
W, w	wheel
Subscripts	
f	front wheel/outrigger
r	rear wheel/outrigger
fr, fl, rr, lr	front right, front left, rear right and rear left, respectively
frx, fry	*x* and *y* components of friction force at front right wheel/outrigger, respectively
flx, fly	*x* and *y* components of friction force at front left wheel/outrigger, respectively
rrx, rry	*x* and *y* components of friction force at rear right wheel/outrigger, respectively
rlx, rly	*x* and *y* components of friction force at rear left wheel/outrigger, respectively